BJRS

BRAZILIAN JOURNAL
OF
RADIATION SCIENCES
10-02A (2022) 01-17

Computational Internal dosimetry of natural cisplatin activated in neutron flux: the Pt-191 contribution

Bussolotti[1,2], G.R., Krstic[3], D., Nikezic[3], D., Leal[1], A.S.,

Zivkovic, M. and Mendes[1], B.M.

[1] *Centro de Desenvolvimento da Tecnologia Nuclear, 31270-901 Belo Horizonte, MG, Brazil*

[2] *Universidade Federal de Minas Gerais, 30130-100 Belo Horizonte, MG, Brazil*

[3] *Department of Physics, Faculty of Sciences, University of Kragujevac, 34000 Kragujevac, R.Domanovic 12, Serbia*

giovanabussolotti@gmail.com

ABSTRACT

Cisplatin is currently used in the treatment of numerous types of tumors, such as head and neck, esophagus, bladder, testicle. However, the cisplatin use is limited due to its cytotoxic effects. Thus, considering its side effects, lines of research are looking for new technologies to reduce the dose of the chemotherapeutic agent needed to control the disease, which may reduce these side effects. The objective of this work was to perform the internal dosimetry of ^{191}Pt radioisotope derived from the activation of natural cisplatin, thus contributing to the evaluation of the feasibility of a new radiopharmaceutical of natural cisplatin activated by neutrons for application in humans. Also, the Pt-191 dosimetry data will be useful for enriched Pt-191 radiopharmaceuticals. The dosimetry was obtained with Monte Carlo simulations using two stylized phantoms developed by Dr. Dragana Krstic and Dr. Dragoslav Nikezic and the ICRP adult reference voxelized phantoms. The highest doses noted in the analytical phantom were in the kidneys (1.58 mGy/MBq), liver (1.32 mGy/MBq), spleen (1.23 mGy/MBq), bladder wall (0.74 mGy/MBq), gallbladder wall (0.56 mGy/MBq), pancreas (0.41 mGy/MBq), and adrenals (0.39 mGy/MBq). For the voxelized phantoms, the highest doses obtained were: kidneys (1.46 mGy/MBq), spleen (1.13 mGy/MBq), liver (1.11 mGy/MBq), gallbladder wall (0.47 mGy/MBq), adrenals (0.41 mGy/MBq), bladder wall (0.36 mGy/MBq), and pancreas (0.29 mGy/MBq). The effective dose was 0.22 mSv/MBq for the analytical phantom, a value similar to that obtained with voxelized phantoms (0.20 mSv/MBq).

ISSN: 2319-0612
DOI: https://10.15392/bjrs.v10i2A.1816
Submitted:2022-01-11
Accepted: 2022-04-25

Keywords: **Cisplatin, internal dosimetry, Monte Carlo.**

1. INTRODUCTION

Cancer is a disease that affects thousands of people every year, and it is expected that in Brazil there will be 625,000 new cases of cancer in the triennium 2020-2022, according to the National Cancer Institute [1]. For men, prostate cancer is the most prevalent neoplasm, with approximately 65,840 new cases in 2020, and breast cancer affected 66,280 women in the same period [1].

Cisplatin is currently used in the treatment of numerous tumors, such as head and neck squamous cell carcinoma, small-cell lung cancer, testicular, bladder, ovarian, breast, brain and other solid cancers [2-4]. It has been proven effective against different types of cancer such as carcinoma, lymphoma, sarcomas, and germ cell tumors [3]. However, its use is limited due to drug resistance and cytotoxic effects such as hepatotoxicity, neurotoxicity, cardiotoxicity, and especially nephrotoxicity [2-4].

Considering the cisplatin adverse effects, lines of research are seeking new technologies to reduce the dose of the chemotherapeutic agent needed to control the disease, potentially reducing the harmful effects. Variations in cisplatin molecule were designed for this purpose, such as Carboplatin, Oxaliplatin, Nedaplatin, Lobaplatin, and Heptaplatin [4]. Similarly, researchers are also looking for technologies that can quantify the cisplatin concentration in the blood as well as its uptake in various organs and tissues of the body, including tumors [5-7]. In vitro and in vivo studies also suggest the possibility of addictive or synergistic radiotherapeutic and chemotherapeutic effect in the use of radiolabeled cisplatin [8-10]. In this manner, this synergy could reduce the amount of cisplatin needed to control the disease and possibly its adverse effects.

The synthesis and the use of some platinum radioisotopes, especially ^{195m}Pt, ^{193m}Pt and ^{191}Pt, to radiolabel cisplatin and similar molecules have been reported previously [5-7, 11-16]. In these previous studies, the researchers have addressed compounds produced based on one enriched platinum radioisotope. The advantage of using only one platinum radioisotope to create the radiopharmaceutical compound is that the dosimetry is easier to calculate since the decay characteristics of a single isotope should be taken in to account in the simulations. However, the feasibility of obtaining radiopharmaceuticals labeled with enriched platinum radioisotopes is low due to the high cost of enrichment.

On the other hand, natural platinum is cheaper than enriched platinum, but it is composed of several natural occurring stable isotopes (^{190}Pt, ^{192}Pt, ^{194}Pt, ^{196}Pt and ^{198}Pt). When activated by neutrons in reactors these stable isotopes produces radioactive isotopes with different decay characteristics such as: ^{191}Pt, ^{193m}Pt, ^{195m}Pt, ^{197}Pt and ^{199}Pt [17]. Chemical separation of these radioisotopes is not possible because they are the same element. Depending on irradiation parameters, the decay time before injection and possibility of chemical purification to remove undesirable radioisotopes like ^{35}S, ^{32}P and ^{199}Au, specially, the ^{191}Pt, ^{193m}Pt, ^{195m}Pt, ^{197}Pt, and ^{35}Cl isotopes will be of major concern for dosimetry of natural cisplatin activate in reactor. Therefore, before conducting clinical tests with molecules containing natural platinum activated in a reactor, the biodistribution and especially the dosimetry of each of these radioisotopes should be studied in order to estimate the absorbed and effective doses that each one of them deliver to the body tissues per unit of injected activity. With these data, it is sufficient to know the activity of each platinum radioisotope injected in to the patient to estimate the absorbed doses due to the whole set of radioisotopes.

The ^{195m}Pt biodistribution was evaluated and published by Sathekge et al. (2013). In their work, using single photon emission tomography (SPECT), the Time-Integrated Activity Coefficient (TIAC) and effective half-life were estimated for the main source-organs: Spleen, Bladder, Liver, Right Kidney, Left Kidney, Blood, and Remaining Organs [5].

In this work, human biodistribution data of ^{195m}Pt-Cipslatin from Sathekge et al. (2013) [5] was adapted for ^{191}Pt. Then, the dosimetry was evaluated using an updated MC code, MCNP6.1 [18], and different human computational models: ICRP adult voxelized phantoms [19] and adult ORNL analytical phantoms [20]. Data generated here will be part of the dosimetry of natural platinum cisplatin activated in reactor. In addition, updated dosimetry data using the ICRP reference voxelized phantoms will be useful to future studies with enriched ^{191}Pt.

2. MATERIALS AND METHODS

Cisplatin irradiated in neutron flux generates various radioisotopes such as ^{191}Pt, ^{193m}Pt, ^{195m}Pt, ^{197}Pt and ^{199}Pt [17]. In this work, ^{191}Pt was chosen for dosimetry evaluation.

The MCNP (Monte Carlo N-Particle) code, version MCNP6.1 [18], was used to perform the energy transport in the cases studied. The simulations were performed using the ICRP 110 reference adult voxelized phantoms [19] and two analytical phantoms developed by the Dr. Dragana Krstic and Dr. Dragoslav Nikezic representing the adults ORNL models [20, 21]. The main characteristics of these models were presented in Table 1. Analytical phantoms (also called Mathematical or Stylized Phantoms) keep a certain similarity in shape and dimensions to the human being. However, they are made up by simple 3D geometric figures described by mathematical equations. On the other hand, voxelized phantoms are constructed by small volumetric pixels (voxels) from medical images such as CT and NMR. In this way, they present a superior anatomical realism [22]. Usually analytical Phantoms are faster in simulations and require less memory to run. These stylized phantom were widely used until the 2000's and they were used to calculate dosimetric data of ICRP compendium about radiopharmaceuticals dosimetry [23].

Table 1: Characteristics of the analytical and voxelized models used in this work [19–21].

Charactristics	**Analytical Models**		**ICRP Voxelized Models**	
	Male	**Female**	**Male**	**Female**
Body weight (kg)	73.7	56.8	70	60
Height (cm)	174	164	176	163
# Organs/tissues	64	65	137	136
# Different Tissue Media	3*	3*	53	53

* Only soft tissue, skeleton and lung

In order to determine the coefficient of the Time-Integrated Activity for the source organs, half-life and uptake data from for ^{195m}Pt-Cisplatin were used [5]. The effective half-life calculation was made from the assumption that ^{195m}Pt and ^{191}Pt have the same biological half-life, due to being the same chemical element in the same molecule. Thus, using Equation 1 and the ^{191}Pt physical half-life [24] it was possible to calculate the ^{191}Pt effective half-life (Table 2).

$$\frac{1}{T_{eff}} = \frac{1}{T_b} + \frac{1}{T_{\frac{1}{2}}} \tag{1}$$

Where, T_{eff} is the effective half-life, T_b is the biological half-life, and $T_{1/2}$ is the physical half-life of the isotope.

Once the ^{191}Pt effective half-life has been calculated, it was possible to obtain the effective decay constant ($\lambda_{Eff.}$) for this radioisotope using the Equation 2:

$$\lambda_{eff} = \frac{ln2}{T_{eff}} \quad (2)$$

Where, λ_{eff} is the decay constant of the radioisotope and T_{eff} is the effective half-life.

Table 2: Effective half-life and effective decay constant data for the various source organs of ^{191}Pt-labeled cisplatin obtained from the biological half-life data of ^{195m}Pt-cisplatin [5] and the physical half-life of ^{191}Pt [24].

Organ	**^{191}Pt**					
	Half Life (s)			**Decay Constant (s^{-1})**		
	$T_{1/2}$	**T_b**	**T_e**	**$\lambda_{Phys.}$**	**$\lambda_{Biol.}$**	**$\lambda_{Eff.}$**
Bloodpool	2.42E+05	3.19E+05	1.38E+05	2.86E-06	2.17E-06	5.03E-06
Liver	2.42E+05	8.86E+05	1.90E+05	2.86E-06	7.82E-07	3.65E-06
Spleen	2.42E+05	8.86E+05	1.90E+05	2.86E-06	7.82E-07	3.65E-06
Right kidney	2.42E+05	8.86E+05	1.90E+05	2.86E-06	7.82E-07	3.65E-06
Left Kidney	2.42E+05	8.86E+05	1.90E+05	2.86E-06	7.82E-07	3.65E-06
Urinary Bladder	2.42E+05	5.18E+05	1.65E+05	2.86E-06	1.34E-06	4.20E-06
Rest	2.42E+05	-1.14E+06	3.07E+05	2.86E-06	-6.07E-07	2.26E-06
Whole body	2.42E+05	1.37E+06	2.06E+05	2.86E-06	5.04E-07	3.37E-06

Setting the injected activity (A_0) as 1Bq and considering the values of percentage uptake in source organs presented in Table 2 originating from the work of Sathekge et al. (2013) [5], it was possible to obtain the initial activity in each source organ (A_{0_organ}) per injected Bq (Table 3). Using Equation 3, the Time-Integrated Activity was calculated from the value of the effective decay constant, determined previously for each source organ.

$$\tilde{A} = \frac{A_0}{\lambda_{Eff}} \tag{3}$$

Where, Ã is the Time-Integrated Activity, which represents the number of radioactive decay in an organ, tissue, or region of the body. The Equation 3 was obtained by integrating the activity equation ($A=A_0.e^{-\lambda_{eff}.t}$) from time 0 to ∞.

The Time-Integrated Activity Coefficient ($\tilde{a}$) for each source organ was calculated using the following equation:

$$\tilde{a} = \frac{\tilde{A}}{A_0} \tag{4}$$

Where, $\tilde{a}$ is the Time-Integrated Activity Coefficient, Ã is Time-Integrated Activity and A_0 is the injected activity [25].

Table 3: Biodistribution data of ^{191}Pt used to obtain the Time-Integrated Activity Coefficient ($\tilde{a}$).

Organ	**Percentage uptake per organ**	**A_{0_organ} per injected Bq** (Bq/Bq)	**Ã** (Bq.s)	**$\tilde{a}$** (s)	**$\tilde{a}$** (h)
Bloodpool	4.0%	3.98E-02	7.90E+03	7.896E+03	2.2
Liver	26.0%	2.60E-01	7.13E+04	7.133E+04	19.8
Spleen	3.0%	3.00E-02	8.23E+03	8.230E+03	2.3
Right Kidney	4.0%	4.00E-02	1.10E+04	1.097E+04	3.0
Left Kidney	4.0%	4.00E-02	1.10E+04	1.097E+04	3.0
Urinary Bladder	8.4%	8.40E-02	2.00E+04	2.000E+04	5.6
Rest	24.0%	2.40E-01	1.06E+05	1.064E+05	33.8
Whole body	84.6%	8.46E-01	2.51E+05	2.512E+05	69.8

To simulate the ^{191}Pt source, two cases were made for each source organ, one case considering the photon decay data and the other, the monoenergetic electron data, this information was made available by the DECDATA® program [24]. A summary of the decay data for this isotope is presented in Table 4.

Table 4: Summary of the ^{191}Pt decay data provided by the DECDATA® program [24].

Radiations	**Emission probability (decay^{-1})**	**Mean Energy (MeV)**
Gamma Ray	0,57	3.50E-01
X-Ray	17,2	5.58E-03
Total photons	***17,77***	-
IC electrons (1)	0,99	5.75E-02
Auger Electrons	13,30	1.34E-03
Total electrons	***14,29***	-

(1) IC- Internal Conversion

We performed 14 cases for each phantom taking into account the emission of photons and electrons, separately, and the source being positioned in different source organs (Right Kidney, Left Kidney, Liver, Spleen, Bladder, Blood and the Remaining Organs) as can be seen for the female analytical model in Figure 1.

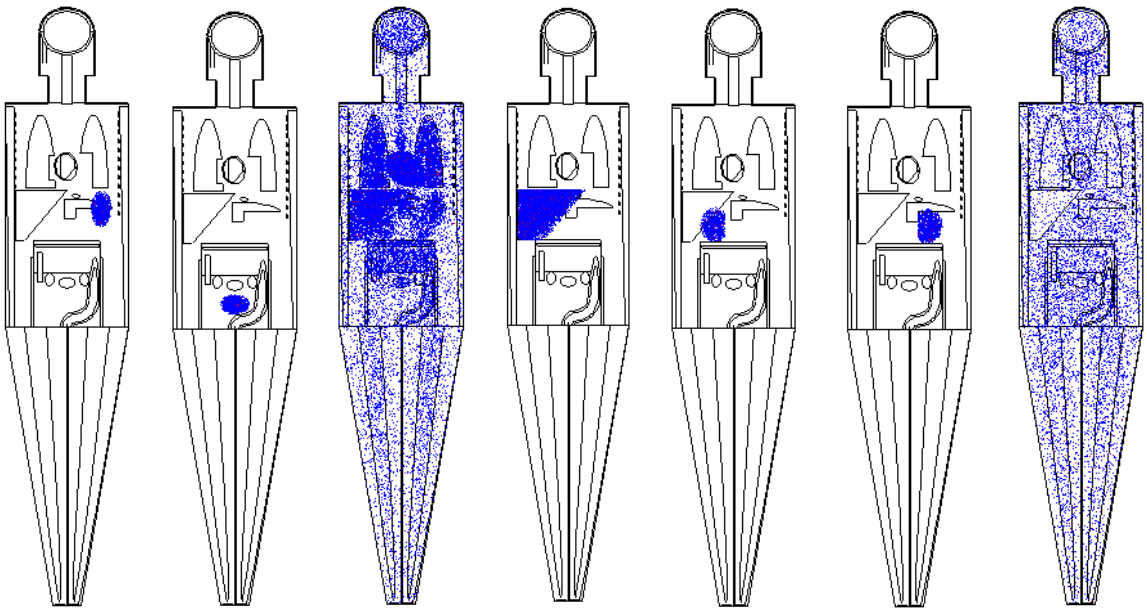

Figure 1: *Source in the female phantom located in the Spleen, Bladder, Blood, Liver, Right Kidney, Left Kidney, and Remaining Organs, respectively.*

In the analytical model it was necessary to perform an approximation of the distribution of blood in the body, due to the fact that it does not have all organs and tissues provided in the ICRP 89 [26]. The blood volume distribution from ICRP 89 [26] was redistributed, weighted by the mass, in the structures present in the phantom. Similarly, the probability of emission in each organ in the model for the source organ called "Remaining Organs" was calculated according to the mass of this set of organs (also weighted by organ mass).

The Tally card specify the quantity that the MC user want to evaluate in the simulation. In this study the tally F6:e was used. This tally returns the mean absorbed dose (MeV/g) in a simulated organ or tissue per particle emitted at the source. For each source organ, the absorbed doses were estimated for all organs and tissues of the model. The program developed in C^{++} extracts the absorbed dose in MeV/g from the output files and converts these values to Gy/particle (photon or electron depending on the simulated case) using the conversion factor 1.602E-10. The absorbed dose per decay was calculated multiplying the values of absorbed dose per particle by the total emission probability of photons or electrons per decay, (Table 4 [24]). The absorbed dose per decay was calculated for photons and electrons for each source organ and then summed to obtain the absorbed dose per decay [27, 28].

The Time-Integrated Activity Coefficient ($\tilde{a}$) represents the total number of nuclear transformations (decays) occurring in each organ per unit of injected activity [25]. The contribution of each source organ to the absorbed dose in each targeted organ in the model was calculated by the product between the total number of decays in such source organ and the absorbed dose per decay. The sum of the contributions from each source organ to a given targeted organ represents the total absorbed dose per unit of injected activity in such target organ.

Secondary particle transport was considered (mode p e). The energy cutoff for photons and electrons was the MCNP6 default (1.0 keV for both). Default electron and photon transport algorithms were used [18]. The number of particle stories followed (NPS) in each simulated case was 2E06. The computer used was an Intel® Xeon® CPU, 4-core, E5-1603 0 @2.80 GHz processor with 8Gb of RAM and 64-bit operating system. The computer time per simulation was about 19 hours.

3. RESULTS AND DISCUSSION

The dosimetric results obtained using the analytical and voxelized phantoms are presented in Table 5 and Table 6. Differences were observed between the estimated absorbed doses using the two types of phantoms (analytic and voxelized).

For the female phantoms, the largest discrepancy occurred in the endosteum, with a difference of 116%. The highest doses noted in the analytical phantom were in the kidneys, liver, spleen, bladder wall, gallbladder wall, pancreas and adrenals in descending order. The highest doses obtained in the voxelized phantom show the same organs, but the order was slightly different: kidneys, spleen, liver, gallbladder wall, adrenals, bladder wall and pancreas.

For the male phantom, the largest discrepancy was found in the thyroid (59%). The highest doses in the analytic phantom were observed in the kidneys, liver, spleen, urinary bladder wall, gallbladder wall and prostate in descending order. For the voxelized phantom, the highest doses were in the kidneys, spleen, liver, gallbladder wall, adrenals and urinary bladder wall.

The effective dose was calculated according to the recommendation of ICRP publication 103, i. e., using the ICRP 103 tissue weighting factors and the sex-averaging effective dose calculated for the male and female phantom [29]. The effective dose result for the analytical phantoms was 0.22 mSv/MBq and for the voxelized phantoms was 0.20 mSv/MBq, with a 10 % difference between these results.

Several works have reported differences between dosimetric results obtained using analytical phantoms or voxelized models [28, 30-32]. An explanation for the observed differences is the anatomical discrepancies among the models. The simplified and geometric shapes of the organs in the stylized phantoms result in larger spaces between the organs than the ones observed in the voxelized phantoms [28, 31]. Such a fact leads to decreased contribution of emissions from adjacent source organs in the absorbed dose from target organs in the analytical phantoms. According to Hadid et al., (2013), this condition can result in absorbed dose differences of one or two orders of magnitude [30]. On the other hand, absorbed doses in walled organs are usually underestimated in voxelized phantoms due to limitations in their resolution. This limitation does not exist for analytical phantoms, and walls as thin as those existing in the human body can be modeled. There are also differences in

the tissue compositions and densities used in the two types of models that may contribute to the observed variations.

Table 5: Absorbed and effective dose per unit of injected activity obtained for the female phantoms.

Organs	**Analytical Phantom**		**Voxelized Phantom**		**Difference(1) (%)**
	Dose [mGy/MBq]	Relative Error	Dose [mGy/MBq]	Relative Error	
Adrenals	0.39	0.019	0.41	0.014	-5%
Endosteum	0.21	0.025	0.10	0.002	116%
Brain	0.07	0.009	0.06	0.005	25%
Breast	0.10	0.012	0.09	0.006	15%
Colon wall	0.24	0.007	0.13	0.005	79%
ET region	0.06	0.549	0.06	0.035	0%
Gallbladder wall	0.56	0.019	0.47	0.015	19%
Heart wall	0.26	0.047	0.16	0.006	63%
Kidneys	1.58	0.002	1.46	0.002	8%
Liver	1.32	0.002	1.11	0.001	19%
Lungs	0.23	0.009	0.15	0.003	53%
Lymphatic nodes	0.14	0.074	0.14	0.010	0%
Muscles	0.09	0.012	0.09	0.001	0%
Esophagus	0.24	0.016	0.15	0.016	63%
Oral Mucosa	0.07	0.502	0.07	0.033	0%
Ovary	0.23	0.031	0.16	0.026	43%
Pancreas	0.41	0.011	0.29	0.006	41%
RBM	0.15	0.014	0.15	0.002	0%
Salivary Glands	0.06	0.312	0.06	0.019	0%
Small intestine wall	0.23	0.005	0.18	0.004	29%
Stomach wall	0.32	0.009	0.24	0.006	33%
Skin	0.09	0.004	0.06	0.003	46%
Spleen	1.23	0.002	1.13	0.003	9%
Thymus	0.15	0.028	0.09	0.028	71%
Thyroid	0.09	0.084	0.08	0.034	15%
Urinary bladder wall	0.74	0.006	0.36	0.010	106%
Uterus/cervix	0.29	0.011	0.21	0.009	36%
Effective dose	0.30	0.011	0.22	0.002	36%

(1)Difference = ((Dose in analytic phantom - Dose in voxelized phantom)/Dose in voxelized phantom)*100

Table 6: Absorbed and effective dose per unit of injected activity obtained for the male phantoms.

Organs	**Analytical Phantom**		**Voxelized Phantom**		**Difference(1) (%)**
	Dose [mGy/MBq]	Relative Error	Dose [mGy/MBq]	Relative Error	
Adrenals	0.17	0.006	0.35	0.016	-51%
Endosteum	0.08	0.014	0.08	0.002	7%
Brain	0.04	0.087	0.05	0.005	-31%
colon wall	0.10	0.326	0.14	0.027	-30%
ET region	0.05	0.034	0.05	0.005	0%
Gallbladder Wall	0.27	0.524	0.40	0.028	-32%
Heart wall	0.11	0.003	0.14	0.014	-18%
Kidneys	0.92	0.048	1.29	0.005	-29%
Liver	0.65	0.003	0.90	0.002	-28%
Lungs	0.10	0.002	0.13	0.001	-27%
Lymphatic nodes	0.12	0.013	0.12	0.003	0%
Muscles	0.07	0.069	0.07	0.009	0%
Esophagus	0.11	0.013	0.13	0.001	-18%
Oral Mucosa	0.06	0.030	0.06	0.016	0%
Testes	0.06	0.480	0.06	0.028	-8%
Pancreas	0.18	0.077	0.25	0.027	-29%
RBM	0.12	0.014	0.12	0.006	0%
Salivary Glands	0.05	0.017	0.05	0.002	0%
Small intestine wall	0.10	0.368	0.14	0.020	-30%
Stomach wall	0.12	0.058	0.18	0.004	-35%
Skin	0.04	0.019	0.05	0.007	-24%
Spleen	0.61	0.023	0.99	0.003	-38%
Thymus	0.08	0.002	0.08	0.003	1%
Thyroid	0.03	0.014	0.07	0.028	-59%
Urinary bladder wall	0.31	0.022	0.35	0.035	-12%
Prostate	0.19	0.012	0.19	0.009	0%
Effective dose	0.14	0.012	0.18	0.002	-26%

(1)Difference = ((Dose Analytic Phantom - Dose Voxelized Phantom) / Dose Voxelized Phantom)*100

Despite the differences found in the absorbed dose, the most exposed organs remain virtually the same. In the case of radiopharmaceuticals for diagnosis, differences such as those observed are not

limiting, and the use of the two models can be interesting, since both have strengths and weaknesses. This is not true for radiopharmaceuticals used for treatment. In this case, personalized dosimetry is indicated.

Areberg et al., (1999) present absorbed dose results for ^{191}Pt, ^{193m}Pt and ^{195m}Pt. In this study, biodistribution data for cisplatin were obtained and SAAM II software was used to perform the dosimetric calculations [11]. The absorbed dose results for the most exposed organs obtained in our work were compared with the values estimated by Areberg et al. (1999) [11]. The graph in Figure 2 illustrates this comparison. In Areberg et al. (1999) study, it is not clear which phantom was used. It is believed, from the date of publication, it may be the Snyder's heterogeneous phantom [33]. Based on this assumption, a comparison with the results of the male phantoms used in this work is more appropriate.

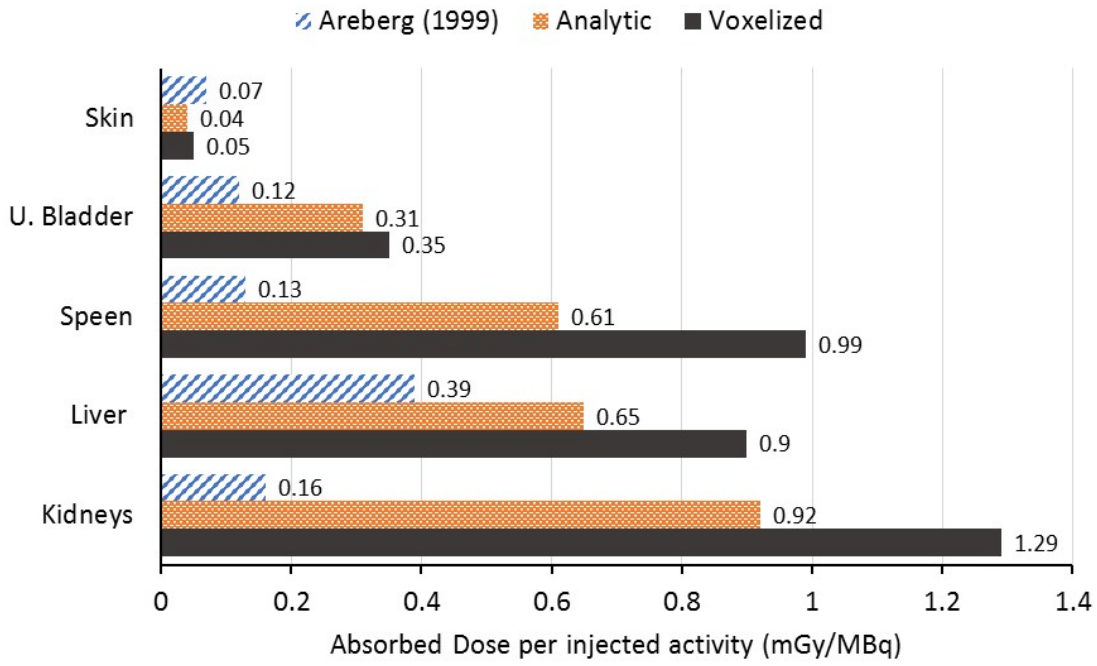

Figure 2: *Comparison graph showing the doses of the analytical phantom of this work, the analytical phantom of Areberg et al., (1999) [11] and the voxelized phantom.*

The effective dose of 0.10 mSv/MBq, reported by Areberg and co-workers (1999) [11], was considerably lower than those obtained in our study (~0.20 mSv/MBq). The ICRP recommendations

for calculating the effective dose were changed in 2007 [29], that change could be another source of the discrepancies. However, as can be seen in Figure 2, the absorbed doses in the most exposed organs reported in the work of Areberg et al. (1999) were systematically lower than the values estimated in this study [11]. One of the factors that could explain such variations could be the difference in the biodistribution data used. However, the study by Areberg et al. (1999) does not mention the Time-Integrated Activity Coefficients used for the source organs [11]. It only mention the references they used to obtain the retention functions. Thus, it cannot be stated with certainty that this was the main reason for the observed underestimates. The use of the SAM II software may also be one of the reasons for the discrepancies since it is a program that can already be considered outdated compared to current Monte Carlo codes.

4. CONCLUSIONS

The dosimetric study using MCNP and different male and female phantoms estimated the absorbed dose per unit activity of injected ^{191}Pt to various organs and tissues. The effective dose per unit of injected activity was also obtained.

The most exposed organs were kidneys, liver, spleen, and bladder, with absorbed doses ranging from 0.5 mGy/MBq to 1.5 mGy/MBq. Small organs close to the source organs such as gallbladder, pancreas, and adrenals also showed relatively high exposure levels. The effective dose per unit activity administered of ^{191}Pt-cisplatin was 0.22 mSv/MBq for the analytical phantoms, a value similar to that obtained with voxelized phantoms (0.20 mSv/MBq).

This work is part of the dosimetric study of natural platinum-labeled cisplatin activated in a nuclear reactor. Future work will address the dosimetry of the isotopes ^{193m}Pt, ^{195m}Pt, ^{197}Pt and ^{35}Cl.

ACKNOWLEDGMENT

The authors thank CNPq for the PIBIC scholarship and CDTN, FAPEMIG, and CNPq for providing the resources and infrastructure that made this work possible.

REFERENCES

[1] INCA, **Estimativa 2020 Incidência de Câncer no Brasil**, 1st ed. Rio de Janeiro - Brasil, 2019. p. 1-122.

[2] ALDOSSARY, S. A. Review on pharmacology of cisplatin: Clinical use, toxicity and mechanism of resistance of cisplatin. **Biomed. Pharmacol. J.**, v. 12(1), p. 7–15, 2019.

[3] DASARI, S. AND TCHOUNWOU, P. B. Cisplatin in cancer therapy: Molecular mechanisms of action. **Eur. J. Pharmacol.**, v. 740, p. 364–378, 2014.

[4] GHOSH, S. Cisplatin: The first metal based anticancer drug. **Bioorg. Chem.**, v. 88, p. 1-21, 2019.

[5] SATHEKGE, M.; WAGENER, J., SMITH, S. V.; SONI, N.; MARJANOVIC-PAINTER, B.; ZINN, C.; VAN DE WIELE, C.; D'ASSELER, Y.; PERKINS, G.; ZEEVAART, J. R. Biodistribution and dosimetry of ^{195m}Pt-cisplatin in normal volunteers. **NuklearMedizin**, v. 52(6), p. 222–227, 2013.

[6] OWENS, S.E.; THATCHER, N.; SHARMA, H.; ADAM, N.; HARRISON, R.; SMITH, A.; ZAKI, A.; BAER, J.C.; MCAULIFFE, C.A.; CROWTHER, D.; FOX, B.W. In vivo distribution studies of radioactively labelled platinum complexes. **Cancer Chemother. Pharmacol.**, v. 14, p. 253–257, 1985.

[7] LANGE, R.C.; SPENCER, R.P.; HARDER, H.C. The antitumor agent cis-$Pt(NH_3)_2Cl_2$: Distribution and dose calculations for ^{193m}Pt and ^{195m}Pt. **J. Nucl. Med.**, v. 14(4), p. 191–195, 1972.

[8] Bodnar, E. N.; Dikiy, M. P.; Medvedeva, E. P. Photonuclear production and antitumor effect of radioactive cisplatin (^{195m}Pt). **J. Radioanal. Nucl. Chem.**, v. 305(1), p. 133–138, 2015.

[9] AREBERG, J. WENNERBERG, J.; JOHNSSON, A.; NORRGREN, K.; MATTSSON, S. Antitumor effect of radioactive cisplatin (^{191}Pt) on nude mice. **Int. J. Radiat. Oncol. Biol. Phys.**, v. 49(3), p. 827–832, 2001.

[10] SOARES, M. A.; MATTOS, J. L. ; PUJATTI, P. B.; LEAL, A. S.; DOS SANTOS, W. G.; DOS SANTOS, R. G. Evaluation of the synergetic radio-chemotherapy effects of the radio labelled cisplatin for the treatment of glioma. **J. Radioanal. Nucl. Chem.**, v. 292(1), p. 61–65, 2012.

[11] AREBERG, J.; NORRGREN, K.; MATTSSON S. Ö. Absorbed doses to patients from ^{191}Pt-, ^{193m}Pt- and ^{195m}Pt-cisplatin. **Appl. Radiat. Isot.**, v. 51(5), p. 581–586, 1999.

[12] SMITH, P. H. S.; TAYLOR, D. M. Distribution and retention of the antitumor agent ^{195}Pt(m)-cis-dichlorodiammine platinum (II) in man. **J. Nucl. Med.**, v. 15(5), p. 349–351, 1974.

[13] DOWELL, J. A.; SANCHO, A. R.; ANAND, D.; WOLF W. Noninvasive measurements for studying the tumoral pharmacokinetics of platinum anticancer drugs in solid tumors. **Adv. Drug Deliv. Rev.**, v. 41(1), p. 111–126, 2000.

[14] AALBERSBERG, E. A.; DE WIT–VAN DER VEEN, B. J.; ZWAAGSTRA, O.; CODÉE–VAN DER SCHILDEN, K.; VEGT, E.; VOGEL, W. V. Preclinical imaging characteristics and quantification of Platinum-195m SPECT. **Eur. J. Nucl. Med. Mol. Imaging**, v. 44(8), p. 1347–1354, 2017.

[15] OBATA, H.; MINEGISHI, K.; NAGATSU, K.; OGAWA, M.; ZHANG, M. R. Synthesis of no-carrier-added [$^{188, 189, 191}$Pt]cisplatin from a cyclotron produced $^{188, 189, 191}PtCl_4^{2-}$ complex. **Sci. Rep.**, v. 11(1), p. 1–7, 2021.

[16] ZEEVAART, J. R. Production of high specific activity ^{195m}Pt-cisplatinum. **Intern. Med. J.**, v. 7(43), p. 14–15, 2013.

[17] LEAL, A. S.; CARVALHO JUNIOR, A.D.; ABRANTES, F. M.; MENEZES, M. A. B. C.; FERRAZ, V.; CRUZ, T. C.; CARDOSO, V. N.; OLIVEIRA, M. C. Production of the radioactive antitumoral cisplatin. **Appl. Radiat. Isot.**, v. 64(2), p. 178–181, 2006.

[18] GOORLEY, J. T.; et al., **MCNP6 User's Manual, Version 1.0, LA-CP-13-00634**. Los Alamos National Laboratory, nº LA-CP-13-00634. p. 765, 2013.

[19] ICRP. Adult Reference Computational Phantoms. ICRP Publication 110. **Ann. ICRP**, v. 39(2), p. 21–45, 2009.

[20] KRSTIĆ, D.; NIKEZIĆ, D. Input files with ORNL-mathematical phantoms of the human body for MCNP-4B. **Comput. Phys. Commun.**, v. 176(1), p. 33–37, 2007.

[21] CRISTY, M.; ECKERMAN, K. F. **Specific Adsorbed Fractions of Energy at Various Ages From Internal Photon Sources**. ORNL/Tm-8381 V1-V7, 1987.

[22] XU, X. G.; ECKERMAN, K. F. **Handbook of Anatomical Models for Radiation Dosimetry**. Florida, USA: Taylor & Francis, 2010.

[23] ICRP. Radiation Dose to Patients from Radiopharmaceuticals: a Compendium of Current Information Related to Frequently Used Substances. ICRP Publication 128. **Ann. ICRP**, v. 44(2)Suppl, p. 7–321, 2015.

[24] ICRP. Nuclear decay data for dosimetric calculations. ICRP Publication 107. **Ann. ICRP**, v. 38(3), p. 7–96, 2008.

[25] BOLCH, W. E.; ECKERMAN, K. F.; SGOUROS, G.; THOMAS, S. R. MIRD pamphlet No. 21: A generalized schema for radiopharmaceutical dosimetry-standardization of nomenclature. **J. Nucl. Med.**, v. 50(3), p. 477–484, 2009.

[26] ICRP. Basic anatomical and physiological data for use in radiological protection: reference values. ICRP Publication 89. **Ann. ICRP**, v. 32(3–4), p. 1–277, 2002.

[27] MENDES, B. M.; FONSECA, T. C. F.; TRINDADE, B. M.; CAMPOS, T. P. R. Desenvolvimento de protocolos de dosimetria interna empregando o código MCNPx e fantomas voxelizados de referência da ICRP 110. **Braz. J. Radiat. Sci.**, v. 01, p. 1–14, 2017.

[28] MENDES, B. M.; FERREIRA, A. V.; NASCIMENTO, L. T. C.; FERREIRA, S. M. Z. M. D.; SILVEIRA, M. B.; SILVA, J. B. New Radiation Dosimetry Estimates for [^{18}F]FLT based on Voxelized Phantoms. **Radiat. Res.**, v. 190(1), 2018.

[29] ICRP. The 2007 Recommendations of the International Commission on Radiological Protection. ICRP Publication 103. v. 37(2-4), p. 1-332, 2007.

[30] HADID, L.; GARDUMI, A.; DESBREÉ, A. Evaluation of absorbed and effective doses to patients from radiopharmaceuticals using the ICRP 110 reference computational phantoms and ICRP 103 formulation. **Radiat. Prot. Dosimetry**, v. 156(2), p. 141–159, 2013.

[31] LEAL, A. S.; BERNARDES, F. D.; MENDES, B. M. Estudo preliminar da dose absorvida e efetiva da cisplatina radiomarcada. **Braz. J. Radiat. Sci.**, v. 8(1), p. 1–15, 2020.

[32] ZANKL, M.; SCHLATTL, H.; PETOUSSI-HENSS, N.; HOESCHEN, C. Electron specific absorbed fractions for the adult male and female ICRP/ICRU reference computational phantoms. **Phys. Med. Biol.**, v. 57(14), p. 4501–4526, 2012.

[33] SNYDER, W. S.; FISHER, H. L.; FORD, M. R.; WARNER, G. G. **MIRD Pamphlet n° 5. Revised - Estimates of absorbed fractions for monoenergetic photon sources uniformly distributed in various organs of a heterogeneous phantom**. New York, USA: Society of Nuclear Medicine, 1978.